A Robust Algorithm for Automated Target Recognition Using Precomputed Radar Cross Sections

Lisa M. Ehrman and Aaron D. Lanterman

Center for Signal and Image Processing
School of Electrical and Computer Engineering
Georgia Institute of Technology, Atlanta, GA 30332, USA

ABSTRACT

Passive radar is an emerging technology that offers a number of unique benefits, including covert operation. Many such systems are already capable of detecting and tracking aircraft. The goal of this work is to develop a robust algorithm for adding automated target recognition (ATR) capabilities to existing passive radar systems.

In previous papers,[1,2] we proposed conducting ATR by comparing the precomputed RCS of known targets to that of detected targets. To make the precomputed RCS as accurate as possible, a coordinated flight model is used to estimate aircraft orientation. Once the aircraft's position and orientation are known, it is possible to determine the incident and observed angles on the aircraft, relative to the transmitter and receiver. This makes it possible to extract the appropriate radar cross section (RCS) from our simulated database. This RCS is then scaled to account for propagation losses and the receiver's antenna gain. A Rician likelihood model compares these expected signals from different targets to the received target profile.

We have previously employed Monte Carlo runs to gauge the probability of error in the ATR algorithm; however, generation of a statistically significant set of Monte Carlo runs is computationally intensive. As an alternative to Monte Carlo runs, we derive the relative entropy (also known as Kullback-Liebler distance) between two Rician distributions. Since the probability of Type II error in our hypothesis testing problem can be expressed as a function of the relative entropy via Stein's Lemma, this provides us with a computationally efficient method for determining an upper bound on our algorithm's performance. It also provides great insight into the types of classification errors we can expect from our algorithm. This paper compares the numerically approximated probability of Type II error with the results obtained from a set of Monte Carlo runs.[3]

Keywords: automatic target recognition, passive radar, coordinated flight model, radar cross section, relative entropy

1. BACKGROUND

Two parallel schools of thought dominate the literature regarding the recognition of fast-moving fixed-wing aircraft. The first proposes a two-step approach to the problem. Target images are created, such as two-dimensional inverse synthetic aperture radar (ISAR) images or a sequence of one-dimensional range profiles.[4] Target recognition is then conducted using these images. The alternate approach has been to bypass the creation of images and attempt recognition directly from the received data. Herman[5,6] takes this second approach to automatic target recognition (ATR), using data obtained from a passive radar system.

Although ATR has been a subject of much research, Herman's application of passive radar was innovative. Unlike traditional radar systems, passive radar systems bypass the need for dedicated transmitters by exploiting "illuminators of opportunity" such as commercial television and FM radio signals. In doing so, they are able to reap a number of benefits. Most notably, the fact that passive radar systems do not emit energy renders them covert. An additional benefit is that the illuminators of opportunity often operate at much lower frequencies than their traditional counterparts. These low-frequency signals are well-suited for ATR.[7–9] Several passive radar systems have been developed in recent years, with Lockheed Martins' Silent Sentry and John Sahr's Manastash Ridge Radar[10,11] being two well-known examples.

(Tel: 404-385-2548. Fax: 404-894-8363. Email: ehrman@ece.gatech.edu, lanterma@ece.gatech.edu)

2. OUR APPROACH

Our approach to the problem falls under the second school of thought regarding ATR. We intend to identify aircraft models using the Radar Cross Section (RCS) obtained from a passive radar system as our key parameter for classification. This is accomplished by comparing the RCS of the true target to the precomputed RCS of known targets in a target library. Since the RCS is the sole parameter for target identification in this scheme, its accurate representation is paramount.

We divide the process of simulating the RCS of known targets into four basic steps. First, we assume that the passive radar system can accurately track the target and provide us with its location. Using the time-correlated aircraft positions, we estimate the aircraft orientation via a coordinated flight model.[12] Given that the aircraft position and orientation are known, we can then compute the incident and observed azimuths and elevations on the aircraft, relative to the transmitter and receiver. Second, using the incident and observed angles, we access an RCS database* containing information for each aircraft in the target class. The appropriate RCS data are extracted from the database, yielding time-correlated RCS profiles for each aircraft in the target class, as though each aircraft is executing the same maneuver as the true target. Next, the RCS profiles are scaled to account for propagation losses, using the Advanced Refractive Effects Prediction System (AREPS). Finally, the profiles are scaled using the Numerical Electromagnetic Code (NEC2) to account for the antenna gain of the receiver. This process results in a set of power profiles simulating those that should arrive at the receiver if each aircraft in the target library were to execute the same maneuver as the true target.

The passive radar system being modeled as part of this research is actually under development by NATO/NC3A. We are proceeding with the intent of eventually comparing our precomputed power profiles to the profiles of targets actually detected by the NATO/NC3A system. Until then, we must simulate the profiles of the true targets. This process is similar to the one just described, with two notable differences. First, when simulating the received data, we use the real aircraft orientation angles rather than those estimated by the coordinated flight model. The second major difference is that we assume the received target profiles are corrupted by noise. The effect of noise on the received power profile is modeled by,

$$P_{RECEIVED} = (\sqrt{P} + w_R)^2 + w_I^2, \tag{1}$$

where P is the power profile prior to being corrupted by noise, and w is zero-mean additive white Gaussian noise, which has real and imaginary components, w_R and w_I.[6] This yields a Rician likelihood model for comparing the received power profile to the precomputed power profiles of targets in the target library. The aircraft type giving the largest likelihood is declared to be the target type.

2.1. Relative Entropy Between Two Ricians

Since the classification scheme is essentially just an M-ary hypothesis testing problem, it seems intuitive that the algorithm's ability to correctly classify the targets is largely determined by the amount of overlap between the target distributions. If the probability density functions of the targets in the target library overlap quite a bit, then the ATR algorithm is expected to have difficulty discriminating between the aircraft; conversely, when the target densities are widely separated, the ATR algorithm should be able to classify the targets with a high rate of success.

Although the ATR algorithm uses an M-ary hypothesis testing scheme, a great deal of insight into the types of classification errors likely to be made by the algorithm is derived by considering several binary discrimination tests. By determining how widely separated any two target densities are, we can estimate the likelihood that one aircraft will be misidentified as another. The relative entropy quantifies this distance between any two target density functions, $p(x)$ and $q(x)$.[13] Since the data points are independent (conditioned on a particular hypothesis) in our case, we can write the relative entropy as the sum of the relative entropy for the original data points using,

*The RCS database was created using the Fast Illinois Solver Code, FISC.

$$D(p(x)||q(x)) = \sum_{i=1}^{N} \left\{ \int_{-\infty}^{\infty} p_i(x_i) \ln \left\{ \frac{p_i(x_i)}{q_i(x_i)} \right\} dx_i \right\}. \tag{2}$$

Given our noise model, it follows that $p(x)$ and $q(x)$ are Rician densities. Thus, they are expressed as

$$p_i(x_i) = \frac{x_i}{\sigma^2} e^{\frac{-(x_i^2+s_{1i}^2)}{2\sigma^2}} I_0 \left\{ \frac{x_i s_{1i}}{\sigma^2} \right\}, \tag{3}$$

and

$$q_i(x_i) = \frac{x_i}{\sigma^2} e^{\frac{-(x_i^2+s_{2i}^2)}{2\sigma^2}} I_0 \left\{ \frac{x_i s_{2i}}{\sigma^2} \right\}. \tag{4}$$

Substituting (3) and (4) into (2) reveals that the relative entropy between two Rician densities with the same σ^2 is

$$D(p(x)||q(x)) = \sum_{i=1}^{N} \left\{ \int_{0}^{\infty} \frac{x_i}{\sigma^2} e^{\frac{-(x_i^2+s_{1i}^2)}{2\sigma^2}} I_0 \left\{ \frac{x_i s_{1i}}{\sigma^2} \right\} \left\{ \frac{s_{2i}^2 - s_{1i}^2}{2\sigma^2} + \ln \left\{ I_0 \left\{ \frac{x_i s_1}{\sigma^2} \right\} \right\} - \ln \left\{ I_0 \left\{ \frac{x_i s_2}{\sigma^2} \right\} \right\} \right\} dx_i \right\}. \tag{5}$$

Two types of errors are possible in a binary hypothesis testing problem. For ease of notation, let us temporarily denote aircraft #1 as the aircraft whose probability density function is $p(x)$; similarly, let us temporarily define aircraft #2 as the target whose probability density function is $q(x)$. The event in which aircraft #1 is misidentified as aircraft #2 is called a Type I error. The probability of such an error is denoted by α. A Type II error occurs if aircraft #2 is mistakenly identified as aircraft #1. Denote the probability of a Type II error as β.

In a Neyman-Pearson scheme, α is set to be some arbitrarily small number, and the decision threshold separating the acceptance regions for aircrafts #1 and #2 shifts to keep α constant as N increases. Within this context, we can use Stein's Lemma[13, 14] to approximate β as

$$\beta_{p(x)||q(x)} \approx e^{-D(p(x)||q(x))}. \tag{6}$$

The subscript on β has been added to clarify which two distributions are being compared. To avoid confusion, the order of $p(x)$ and $q(x)$ in the subscript is kept consistent with the order in the definition of $D(p(x)||q(x))$. Using this notation, $\beta_{p(x)||q(x)}$ is the probability that aircraft #2 (whose density is $q(x)$) will be misidentified as aircraft #1 (whose density is $p(x)$).

In later sections, we compute β for each possible aircraft pairing. Since our target library is currently comprised of four targets, this results in a total of sixteen ordered pairings. The order of the pairing does matter; it should be clear from examining (5) that the relative entropy for this problem is not symmetric. Note that in (5), the x_i parameter is the dummy variable of the integral. This implies that we do not actually need to substitute in the power profile of a particular true target; rather, x_i is swept from zero to infinity. As a consequence, there is no need for Monte Carlo runs when computing the relative entropy. This significantly reduces the computational complexity involved in determining algorithm performance.

2.2. Anticipated Noise Levels

The only parameter in (5) yet to be determined is the noise power, σ^2. This is expressed in dBW as,

$$P_N = \frac{kT_0N_F}{CPI}, \tag{7}$$

where k is Boltzmann's constant, T_0 is temperature in Kelvin, N_F is the unitless noise figure, and CPI is the coherent processing interval of the system.[15] To match the NATO system, the CPI is set equal to 0.5 seconds, and T_0 is set equal to 290 K. Determining the appropriate noise figure of the system is more difficult. In an urban environment, a reasonable upper bound on the noise figure due to thermal noise and out-of-band interference might be 30 dB. However, transmitter interference must also be addressed. Typically, the direct path interference manifests itself as a spike in the cross-ambiguity function. Since the transmitter's power and location are known, and since the direct path interference spike occurs along the axis with zero velocity, this spike can usually be identified and removed. The more treacherous effect of the transmitter interference is that it can raise the "thumbtack" noise floor of the ambiguity function, potentially masking a target spike. To be thorough, this should also be considered when computing the noise figure.

If the ambiguity function is normalized such that the direct path spike has unit height, then the average pedestal height, or sideband power, is given by

$$P_{pedestal} = \frac{1}{B \times CPI}, \tag{8}$$

where B is the signal bandwidth, and CPI is the coherent processing interval.[16] To match the NATO/NC3A system, values of 45 kHz and 0.5 seconds are used for B and CPI, respectively.

If propagation losses and antenna gain are neglected, the pedestal power is 44 dBW below the direct-path spike. Since the illuminator of opportunity exploited by the NATO/NC3A system has a power level of 50 dBW, the sideband power is 6 dBW. Propagation losses and antenna gain play a significant role, lowering the pedestal power by 95 dBW. The electronics in the receiver of the NATO/NC3A system also mitigate the problem by suppressing the direct path signal by 70 dBW, which reduces the sideband power to -159 dBW. More sophisticated filters could be implemented to further reduce the noise figure, but using the specifications of the system being modeled, the effective noise figure falls between 40 and 45 dB. Thus, the effects due to transmitter interference are far more significant than those due to thermal noise and out-of-band interference.

This underscores an important point. In the interest of gauging the algorithm's performance in the presence of noise, the results presented in Section 3 correspond to a broad range of noise figures. When reading that section, it is imperative to recall that the anticipated noise figure in the real system is only 40 dB.

3. RESULTS

A series of maneuvers are used to test the ATR algorithm. The first maneuver is simply a straight-and-level flight path in which the aircraft flies directly away from the receiver at a speed of 200 m/s and an altitude of 8000 m AGL (above ground level). The second maneuver is nearly identical to the first, but the aircraft heading is rotated 90^o so that the aircraft flies broadside to the receiver. This provides the receiver with a wider array of observed azimuths on the aircraft. The third encounter was recorded on-board a maneuvering F-15[†], providing us with a more difficult test of our algorithm. All three maneuvers are conducted approximately 30 km from the receiver, and are located in the receiver's main lobe.

[†]The F-15C trajectory was obtained, courtesy of Major Larkin Hastriter and Lt. Col. Adam MacDonald, from the Joint Helmet Cuing System, Mission JH-16, conducted by the 445th Flight Test Squadron at Edwards Air Force Base in May 2000.

3.1. Straight-and-Level Trajectory #1

The precomputed power profiles corresponding to the first straight-and-level trajectory are shown in Figure 1a. Recall that this maneuver involves the aircraft flying directly away from the receiver. Since the range of aspects of the aircraft presented to the receiver is very limited, it is not surprising that the power profiles of all four aircraft look very similar. Four hundred Monte Carlo runs are conducted at each noise figure in the study, with a quarter of the runs corresponding to each aircraft being the true target. The noise figure is swept from 30 dB to 100 dB in increments of 5 dB. As mentioned in Section 2.2, the noise figure is swept well beyond the anticipated noise levels so that we can witness the breaking point of the algorithm. The probability of error determined by the Monte Carlo runs is shown in Figure 1b. The similarities among the probability-of-error curves of the four aircraft corroborate the point that the precomputed power profiles are quite similar.

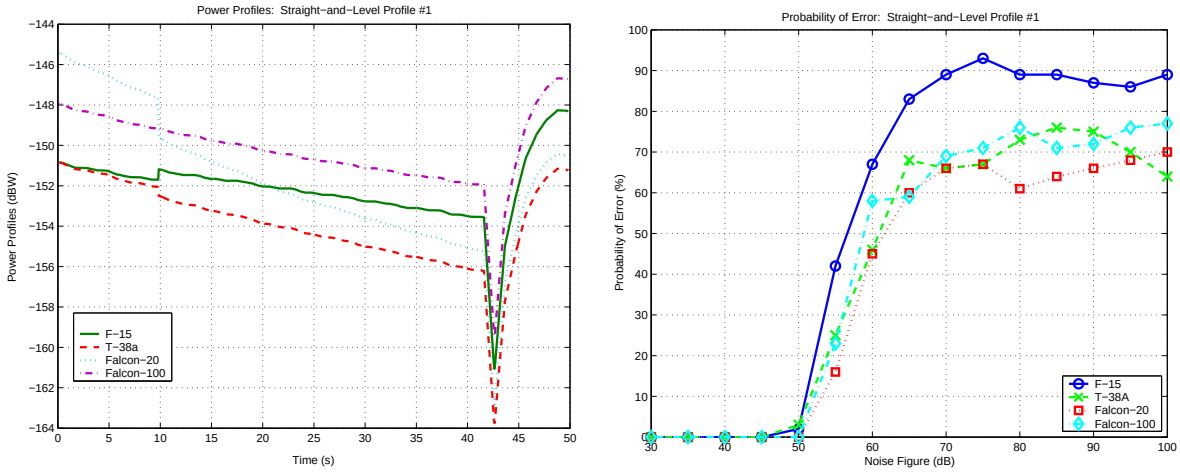

Figure 1. Straight-and-Level Trajectory #1: a.) Power Profiles (left), b.) Probability of Error Vs. Noise Figure (right)

Confusion matrices are tabulated to provide additional insight into the types of identification errors exhibited by the algorithm. The confusion matrices for the first straight-and-level maneuver at noise levels of 55 and 60 dB are shown in Tables 1 and 2. The aircraft listed in the first column correspond to the true target. The aircraft listed across the top row pertain to the aircraft chosen by the algorithm.

Several conclusions may be drawn from the probability of error curves and confusion matrices. For example, the algorithm performs perfectly until the noise figure reaches 50 dB.[‡] By 70 dB, the probability of error, averaged over all four aircraft, approaches 75%. Since there are four aircraft in the study, this is equivalent to chance. The confusion matrices also provide insight into the likeliest misidentifications made by the algorithm. For example, they indicate that if an aircraft is misidentified as the F-15, then the true target is likeliest to have been a T-38A. The probabilities that it was actually a Falcon-100 or Falcon-20 are lower. Similarly, when the algorithm mistakenly chooses an aircraft as the T-38A, it is likeliest that the true target was really the F-15. Under these circumstances, the probability that it was actually a Falcon-100 or Falcon-20 is lower. We can also deduce that the Falcon-100 is most likely to be the true target when the algorithm mistakenly chooses an aircraft as the Falcon-20. The F-15 and T-38A had similar probabilities of being the true target in this setting, but had lower probabilities than the Falcon-100. Finally, when the algorithm mistakenly chooses the Falcon-100, the F-15 is the likeliest to be the true target, followed by the Falcon-20 and T-38A.

Equation 6 is used to approximate β for each possible target pairing; these results, shown in Figure 2, are compared to the results of the Monte Carlo runs. For example, Figure 2a shows the probability that each aircraft will be misidentified as the F-15. Similar findings are given in Figures 2b, 2c, and 2d for the T-38A,

[‡]We would not actually expect the algorithm to perform perfectly in a real setting, as there may be factors that we have neglected to model. However, the simulation results do indicate that the algorithm would perform well at low noise levels.

Table 1. Confusion matrix for straight-and-level trajectory #1 with noise figure = 55 dB. The aircraft listed in the first column correspond to the true target. The aircraft listed across the top row pertain to the aircraft chosen by the algorithm.

Aircraft	F-15	T-38A	Falcon-20	Falcon-100
F-15	58	24	3	15
T-38A	21	75	3	1
Falcon-20	1	5	84	10
Falcon-100	14	3	6	77

Table 2. Confusion matrix for straight-and-level trajectory #1 with noise figure = 60 dB.

Aircraft	F-15	T-38A	Falcon-20	Falcon-100
F-15	33	34	13	20
T-38A	20	54	13	13
Falcon-20	10	19	55	16
Falcon-100	22	13	23	42

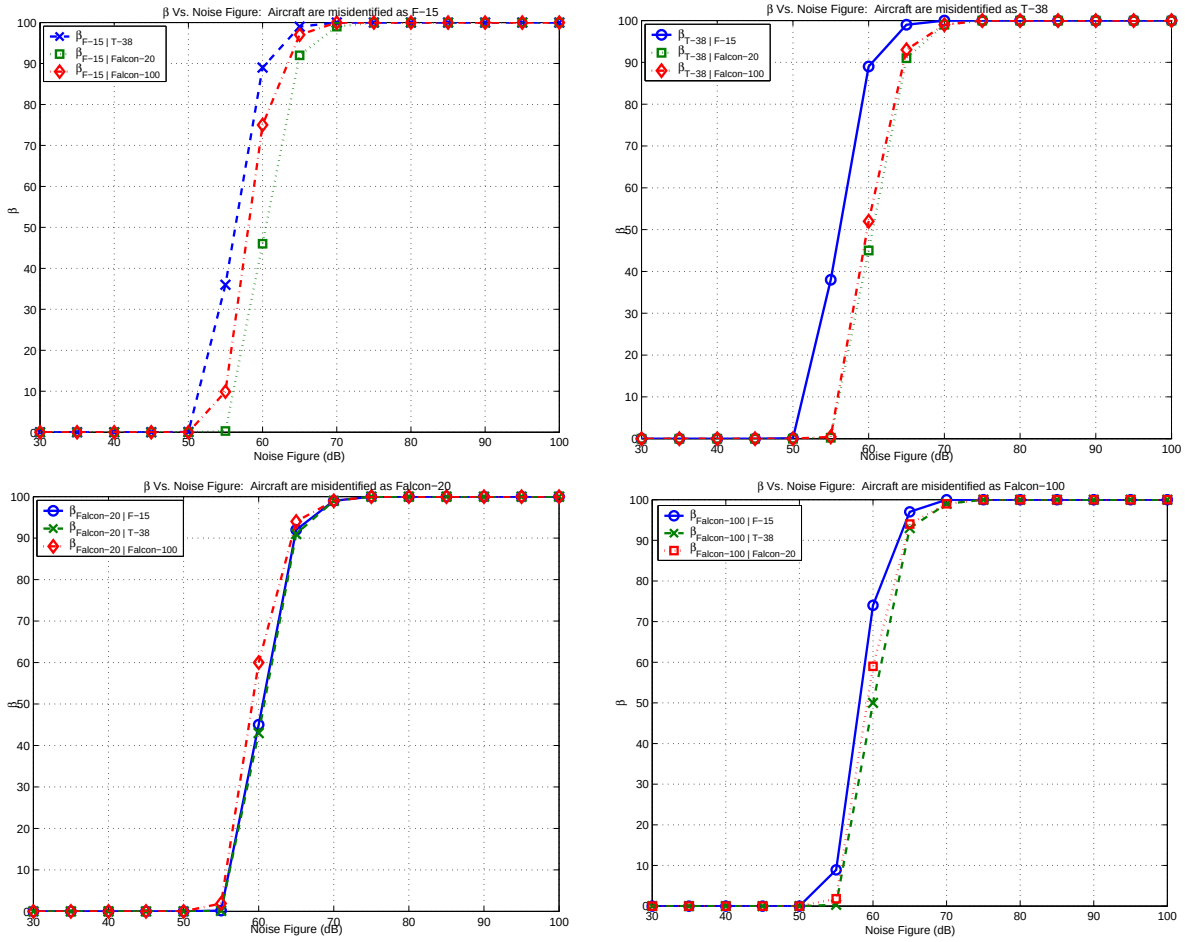

Figure 2. Straight-and-Level Trajectory #1: β Vs. Noise Figure when targets are mistakenly chosen to be the: a.) F-15 (top left), b.) T-38A (top right), c.) Falcon-20 (bottom left), d.) Falcon-100 (bottom right)

Falcon-20, and Falcon-100, respectively. If β is viewed as an upper bound on the algorithm's performance, then it corroborates every one of the trends observed in the Monte Carlo runs. This includes the observation that the probability of error approaches chance when the noise figure reaches 70 dB. This implies that the target distributions overlap almost entirely, which means that β approaches 100% for an infinitesimally small α.

3.2. Straight-and-Level Trajectory #2

The analysis is repeated for the second straight-and-level maneuver. Recall that the aircraft now fly broadside to the receiver. Thus, a much wider range of aspects are presented to the receiver. The manifestation of this is evident in the power profiles, shown in Figure 3a. They look much less similar in shape and amplitude than before. This leads us to anticipate much better performance than was observed in the previous maneuver.

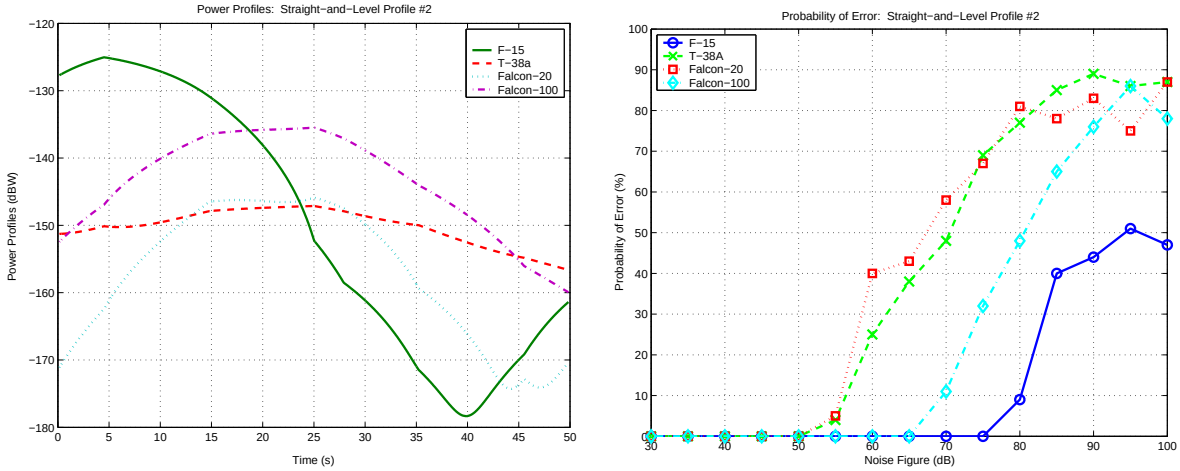

Figure 3. Straight-and-Level Trajectory #2: a.) Power Profiles (left), b.) Probability of Error Vs. Noise Figure (right)

The probability of error curves derived from the Monte Carlo runs, shown in Figure 3b, confirm this suspicion. No errors occur until the noise figure reaches 55 dB, and at this point, they are limited to the T-38A and Falcon-20. The probability of error remains at zero for the Falcon-100 until the noise figure hits 70 dB, and remains at zero for the F-15 until the noise figure reaches 80 dB. Confusion matrices confirming these trends appear in Tables 3, 4, and 5 for noise figures of 55, 70, and 80 dB.

Table 3. Confusion matrix for straight-and-level trajectory #2 with noise figure = 55 dB.

Aircraft	F-15	T-38A	Falcon-20	Falcon-100
F-15	100	0	0	0
T-38A	0	96	4	0
Falcon-20	0	5	95	0
Falcon-100	0	0	0	100

Several conclusions are drawn from this experiment. First, the probability of error curves and confusion matrices suggest that the only errors made for noise figures less than 70 dB pertain to swapping the T-38A and Falcon-20. Not only are the Falcon-100 and F-15 never misidentified when they are the true targets; they are never mistakenly chosen when the true target is the T-38A or Falcon-20. Once the noise figure reaches 70 dB, the Falcon-100 begins being misidentified when it is present, and mistakenly chosen when it is not. Neither of these two events occur with the F-15 until the noise figure reaches 80 dB. The computation of β, presented in Figure 4, is in accord with every one of these conclusions.

Table 4. Confusion matrix for straight-and-level trajectory #2 with noise figure = 70 dB.

Aircraft	F-15	T-38A	Falcon-20	Falcon-100
F-15	100	0	0	0
T-38A	0	52	40	8
Falcon-20	0	50	42	8
Falcon-100	0	2	9	89

Table 5. Confusion matrix for straight-and-level trajectory #2 with noise figure = 80 dB.

Aircraft	F-15	T-38A	Falcon-20	Falcon-100
F-15	91	3	0	6
T-38A	16	23	19	42
Falcon-20	15	24	19	42
Falcon-100	17	17	14	52

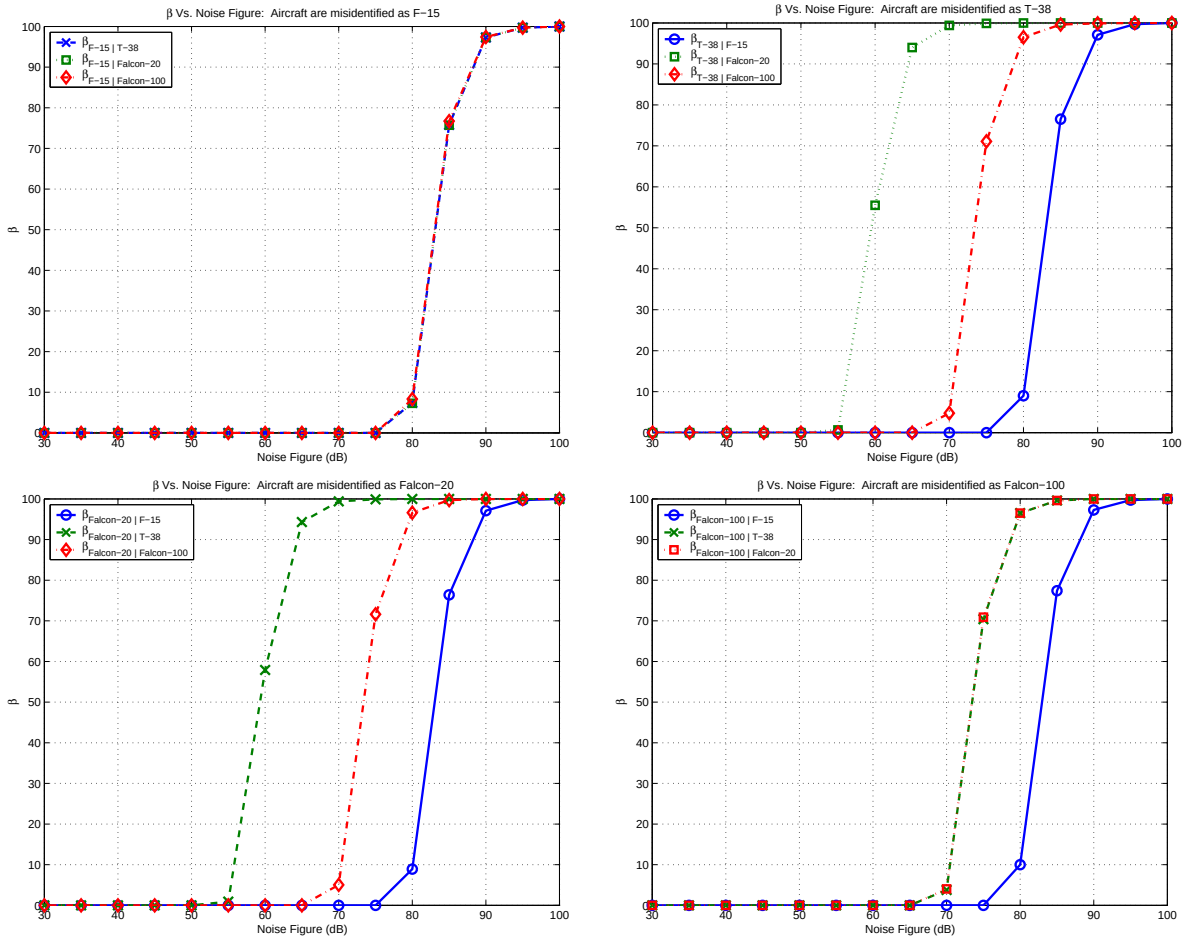

Figure 4. Straight-and-Level Trajectory #2: β Vs. Noise Figure when targets are mistakenly chosen to be the: a.) F-15 (top left), b.) T-38A (top right), c.) Falcon-20 (bottom left), d.) Falcon-100 (bottom right)

3.3. Edwards Maneuver

The final test of the algorithm uses a much more difficult maneuver than the previous two tests. This maneuver is shown in both a 3-D perspective and a God's eye view in Figure 5. Note that this test involves changes in aircraft heading, pitch, and roll.

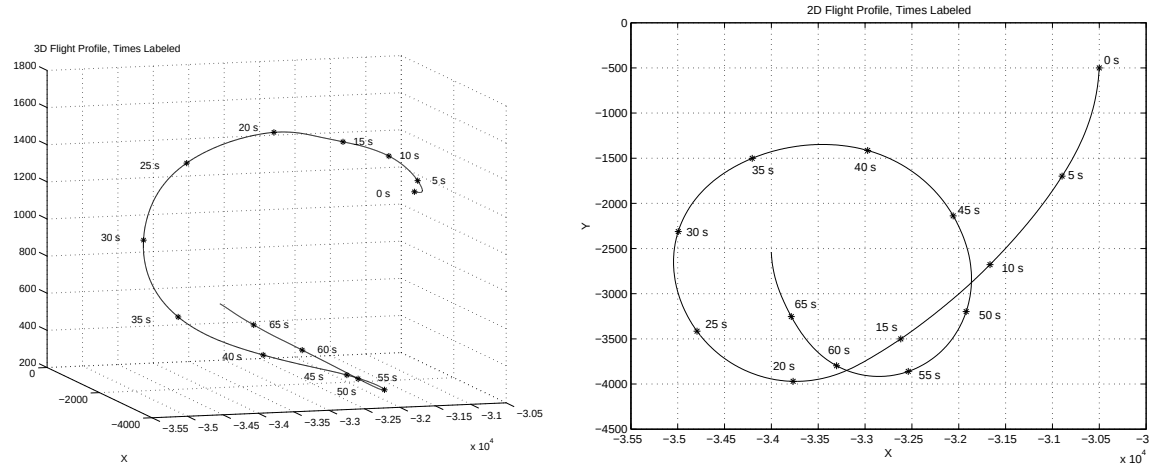

Figure 5. F-15 maneuver: a) 3-D view (left), b) top view (right).

The precomputed power profiles for this maneuver are shown in Figure 6a. The corresponding Monte Carlo probabilities of error are shown in Figure 6b. This time, the shapes of the power profiles vary, but the amplitude of the profiles is fairly similar for all four aircraft models. Confusion matrices are given in Tables 6 and 7 for noise figures of 60 and 70 dB.

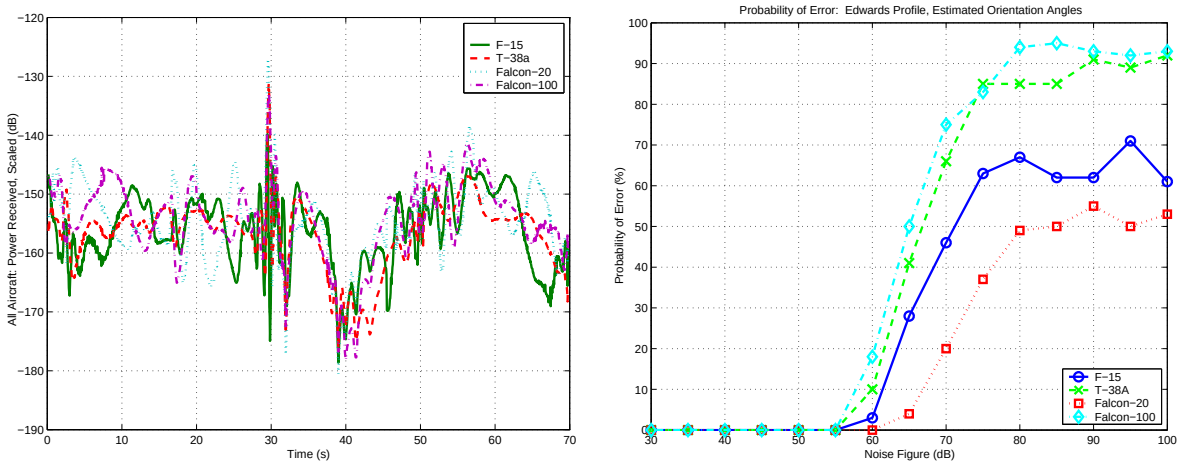

Figure 6. Edwards Trajectory: a.) Power Profiles (left), b.) Probability of Error Vs. Noise Figure (right)

Once again, the probability of error curves and confusion matrices provide us with ample data for making conclusions. This time, no identification errors are recorded until the noise figure reaches 60 dB. The algorithm fails to be effective once the noise figure reaches 80 dB. If a true target is misidentified as the F-15, it was likeliest to have been the T-38A or Falcon-100, with the probability that it was the Falcon-20 being somewhat smaller. Similarly, if the T-38A is mistakenly identified as present when it is not, the true target was most likely the Falcon-100. The Falcon-20 was the least likely aircraft to be present when the algorithm mistakenly identified

Table 6. Confusion matrix for the Edwards trajectory with noise figure = 60 dB

Aircraft	F-15	T-38A	Falcon-20	Falcon-100
F-15	97	1	0	2
T-38A	2	90	0	8
Falcon-20	0	0	100	0
Falcon-100	1	17	0	82

Table 7. Confusion matrix for the Edwards trajectory with noise figure = 70 dB

Aircraft	F-15	T-38A	Falcon-20	Falcon-100
F-15	54	16	16	14
T-38A	27	34	22	17
Falcon-20	10	7	80	3
Falcon-100	30	24	21	25

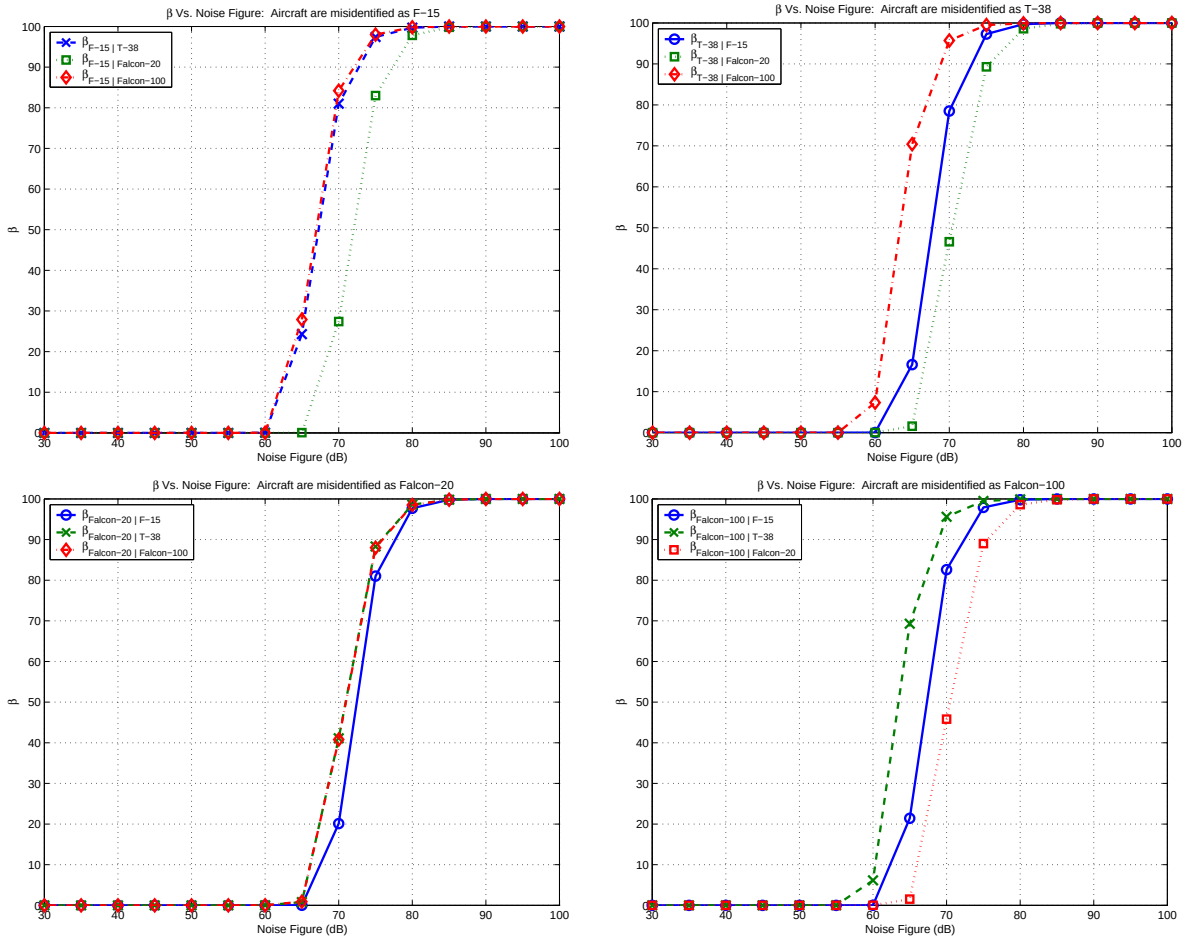

Figure 7. Edwards Trajectory: β Vs. Noise Figure when targets are mistakenly chosen to be the: a.) F-15 (top left), b.) T-38A (top right), c.) Falcon-20 (bottom left), d.) Falcon-100 (bottom right)

the true target as the T-38A. A similar trend is noticeable when the true target is mistakenly identified as the Falcon-100. This time, the T-38A was the most likely aircraft to be the true target, followed by the F-15. Finally, when the Falcon-20 is falsely matched with the true target, the Falcon-100 and T-38A were equally likely to be the true target. The probability that the true target was an F-15 is slightly lower. As before, the plots of β, shown in Figure 7, are in accord with every one of these conclusions.

4. CONCLUSIONS

Two major conclusions can be drawn from this work. First, the simulations suggest that the algorithm will perform very well at the anticipated noise levels. In fact, every one of the simulations resulted in perfect identification of all four aircraft for noise figures below 50 dB. While we do not want to suggest that a real system would function perfectly, as there may be phenomena present in a real system that have not been modeled, the findings do suggest that the real system should perform well at the anticipated noise levels. The data presented in this paper also suggest that β, computed in term of the relative entropy, provides a way to gauge system performance that is both reliable and computationally efficient. Further work will seek to extend this idea to a Bayesian framework by computing Chernoff information.

ACKNOWLEDGMENTS

This work was sponsored by the NATO Consultation, Command, and Control Agency (NC3A) and Air Force Office of Scientific Research (AFOSR) grant F49620-03-1-0340. The authors would like to thank Dr. Paul Howland and Dr. Rene van der Heiden at NC3A for their support. We are also indebted to Major Larkin Hastriter and Lt. Col. Adam MacDonald for their assistance in obtaining aircraft flight paths.

REFERENCES

1. L. Ehrman and A. Lanterman, "Automated target recogntion using passive radar and coordinated flight models," in *Automatic Target Recognition XIII*, **SPIE Proc. 5094**, (Orlando, FL), April 2003.
2. L. Ehrman, *Automatic Target Recognition Using Passive Radar and a Coordinated Flight Model*, Master's Thesis, School of Electrical and Computer Engineering, Georgia Institute of Technology, Atlanta, GA, 2003.
3. L. Ehrman and A. Lanterman, "Target identification using modeled radar cross sections and a coordinated flight model," in *Proceedings from the Third Multi-National Conference on Passive and Covert Radar*, (Seattle, WA), October 2003.
4. S. Jacobs and J. O'Sullivan, "Automatic target recognition using sequences of high resolution radar range-profiles," *IEEE Trans. on Aerospace and Electronic Systems* **36**(2), pp. 364–382, 2000.
5. S. Herman, *A Particle Filtering Approach to Joint Passive Radar Tracking and Target Classification*, Doctoral Dissertation, Department of Electrical and Computer Engineering, Univ. of Illinois at Urbana-Champaign, Urbana, IL, 2002.
6. S. Herman and P. Moulin, "A particle filtering approach to joint radar tracking and automatic target recognition," in *Proc. IEEE Aerospace Conference*, (Big Sky, Montana), March 10-15 2002.
7. Y. Lin and A. Ksienski, "Identification of complex geomtrical shapes by means of low-frequency radar returns," *The Radio and Electronic Engineer* **46**, pp. 472–486, Oct. 1976.
8. H. Lin and A. Ksienski, "Optimum frequencies for aircraft classification," *IEEE Trans. on Aerospace and Electronic Systems* **17**, pp. 656–665, Sept. 1981.
9. J. Chen and E. Walton, "Comparison of two target classification techniques," *IEEE Trans. on Aerospace and Electronic Systems* **22**, pp. 15–21, Jan. 1986.
10. J. Sahr and F. Lind, "The Manastash ridge radar: A passive bistatic radar for upper atmospheric radio science," *Radio Science* , pp. 2345–2358, Nov.-Dec. 1997.
11. J. Sahr and F. Lind, "Passive radio remote sensing of the atmosphere using transmitters of opportunity," *Radio Science* , pp. 4–7, March 1998.
12. L. Ehrman and A. Lanterman, "Estimation of aircraft orientation from flight paths using a coordinated flight model," *submitted to IEEE Transactions on Aerospace and Electronic Systems* , November 2002.
13. T. M. Cover and J. A. Thomas, *Elements of Information Theory*, John Wiley & Sons, Inc., 1991.

14. A. D. Lanterman, J. A. O'Sullivan, and M. I. Miller, "Kullback-Liebler distances for quantifying clutter and models," *Optical Engineering* **38**, pp. 2134–2146, December 1999.
15. D. Barton, *Modern Radar System Analysis*, Artech House, 1988.
16. M. A. Ringer, G. J. Frazer, and S. J. Anderson, "Waveform analysis of transmitters of opportunity for passive radar," *Surveillance Systems Division, Electronics and Surveillance Research Laboratory* .